Description and Uncertainty Analysis of NIST's
20 Liter Hydrocarbon Liquid Flow Standard (20 L HLFS)

Aaron N. Johnson
NIST Fluid Metrology Group
100 Bureau Drive
Gaithersburg, MD 20899
301-975-5954
Aaron.Johnson@nist.gov

TT Yeh
NIST Fluid Metrology Group
100 Bureau Drive
Gaithersburg, MD 20899
301-975-5953
TT.Yeh@nist.gov

Chris J. Crowley
NIST Fluid Metrology Group
100 Bureau Drive
Gaithersburg, MD 20899
301-975-4648
Chris.Crowley@nist.gov

Abstract: The National Institute of Standards and Technology (NIST) uses a bi-directional piston prover as its primary standard for measuring hydrocarbon liquid flows ranging from 1.86×10^{-5} m^3/s (0.3 gpm) to 2.6×10^{-3} m^3/s (40 gpm). An uncertainty analysis is presented that shows that the uncertainty over this flow range is 0.074 % ($k = 2$). As a verification of the uncertainty analysis NIST shows comparison results between its new 20 L piston prover standard and its other hydrocarbon liquid standards and its water flow standard using a dual rotor turbine meter as the transfer standard.

Keyword: NIST liquid hydrocarbon flow standard, piston prover, water draw procedure, liquid flow calibration, uncertainty analysis, 20 L HLFS

1. Introduction

NIST measures liquid hydrocarbon flows using the four primary standards listed in Table 1. NIST's customers establish traceability to the SI unit of flow by calibrating a meter under test (MUT) against these U.S. national standards. The standards are designed to accommodate all types of pulse producing flowmeters, although turbine meters are the most frequently calibrated at NIST. The first two standards (*i.e.*, the Small and Large Cox Bench) work on a gravimetric principle whereby the flow is determined by weighing the mass of liquid collected in a tank over a measured time interval. The latter two primary standards are the 2 L Hydrocarbon Liquid Flow Standard (2 L HLFS) and the newly developed 20 L Hydrocarbon Liquid Flow Standard (20 L HLFS). These piston prover standards work on a volumetric principle whereby the piston displaces a known volume of fluid in a measured time interval. The first three standards in the table have been in use for several years and their operation and uncertainty analyses are documented in NIST internal records and in previous publications [1, 2]. In the current manuscript we document the operating principle for the 20 L HLFS, its governing flow equations, calibration procedure, uncertainty analysis, and inter-comparison results with the three other NIST standards and with NIST's Water Flow Facility [3].

Table 1. *Capabilities of NIST's four Hydrocarbon Liquid Flow Standards. Flow standards are used with Stoddard solvent (i.e., MIL-C-7024 B Type II) or fluids with identical kinematic viscosities.[a, b]*

NIST Primary Flow Standard	Flow Range	Expanded Uncertainty		Pressure Range	Temperature Range
		Volumetric Flow	Mass Flow		
Small Cox Bench	0.05 to 8 lpm (0.014 to 2.1 gpm)	0.12 %	0.12 %	150 kPa to 250 kPa	14ºC to 30ºC
Large Cox Bench	5.3 to 918 lpm (1.4 to 242 gpm)	0.12 %	0.12 %	150 kPa to 250 kPa	14ºC to 30ºC
2 L HLFS (small piston prover)	0.19 to 5.7 lpm (0.05 to 1.5 gpm)	0.04 %	0.05 %	150 kPa to 315 kPa	21ºC to 23ºC
20 L HLFS (medium piston prover)	1.1 to 151 lpm (0.3 to 40 gpm)	0.074 %	0.08 %	150 kPa to 315 kPa	21ºC to 23ºC

2. NIST's 20 L HLFS

2.1. Description of the 20 L HLFS


(a)

(b)
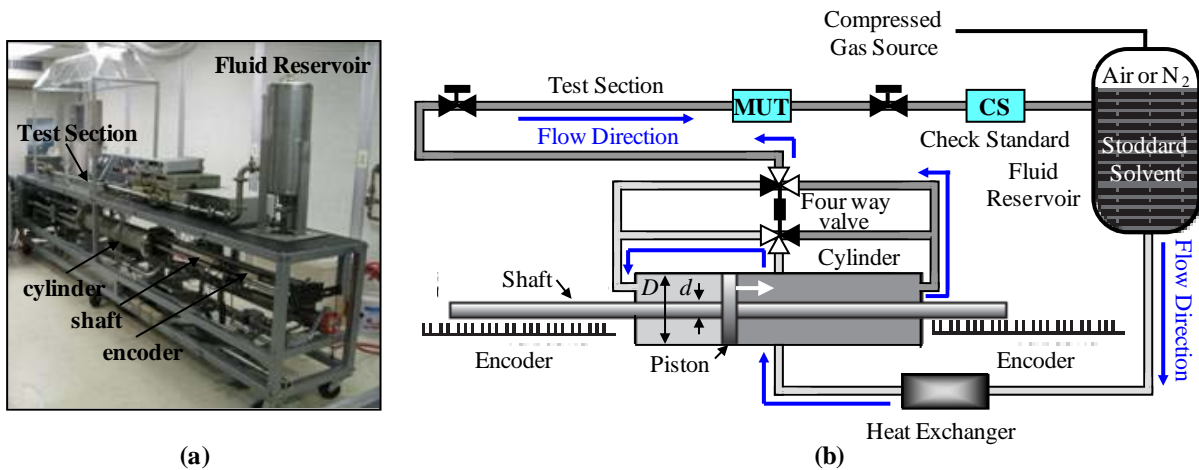
Figure 1. *Photograph and drawing of the essential components of the 20 L HLFS*

---

[a] Throughout this document the units lpm are actual liters per minute. Divide lpm by 60000 to convert to m^3/s and divide lpm by 3.785412 to convert to gallons per minute which is herein abbreviated by gpm.

[b] Uncertainty values at approximately the 95 % confidence interval having a coverage factor of two ($k = 2$). These uncertainties do not include repeatability, reproducibility, and hysteresis of the flowmeter being calibrated. These additional uncertainty components are assessed during a flowmeter calibration and are documented in a report of calibration.

The photograph in Fig. 1a shows the major components of the 20 L HLFS and the diagram in Fig. 1b shows the flow path of the calibration fluid throughout the prover assembly when the piston is stroking to the right. As the piston strokes rightward the flow exits the cylinder on the right side and moves through the upper section of the four-way valve into the test section. The MUT is calibrated using the known flow delivered from piston-cylinder assembly as the reference. The data collected during a flowmeter calibration is verified against a turbine meter check standard installed downstream of the MUT. Fluid leaving the test section enters into a fluid reservoir where a compressed gas source is used to pressure the fluid. The fluid pressure helps prevent cavitation on the turbine meter blades of NIST's check standard as well customer turbine meters. As the flow exits the reservoir it is directed through a heat exchanger and then around the piston-cylinder assembly to the lower section of the four-way valve. The flow loop is completed when the fluid reenters the left side of the cylinder. Flow continues to accumulate in the left side of the cylinder until the piston reaches the end of the rightward stroke, at which time the four-way valve is actuated and the piston strokes leftward. As observed in the Fig. 2, the four-way valve maintains unidirectional flow in the test section regardless of the direction of the piston stroke.
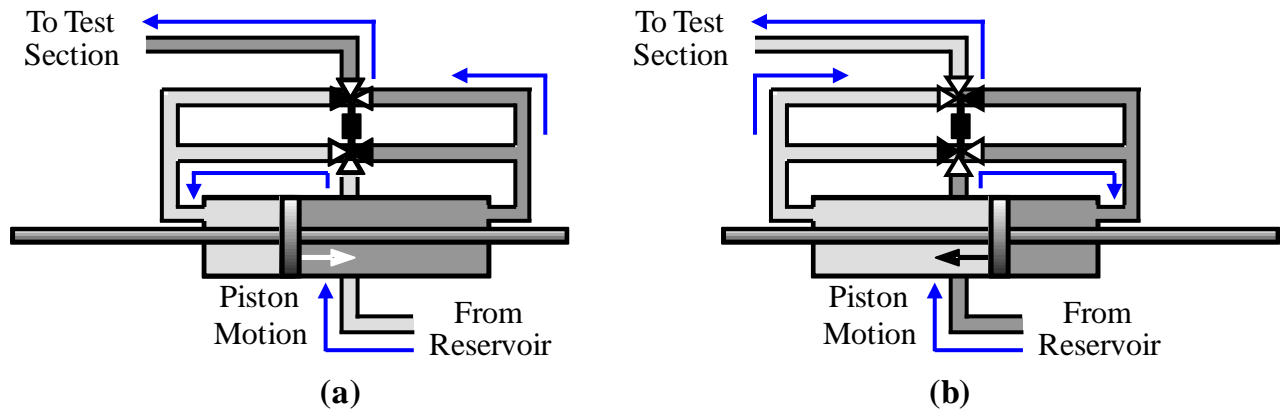
Figure 2. *Sketch showing the four-way valve positions and the corresponding flow directions for the piston stroking rightward (a) and leftward (b)*

The piston is driven using a servomotor and drive gear system that is coupled to the piston shaft. Calibration data is collected only after a feedback circuit controls the servomotor output so that the piston velocity reaches a constant value equal to the desired flow set point divided by the cross sectional area. A timing circuit measures the duration of the piston stroke (Δt) while the distance is measured redundantly by two linear encoders both with a nominal encoder constant of $\Delta L'_e = 20 \ \mu\text{m/pulse}$ (or 50 pulses/mm). The length of the piston stroke is the encoder constant multiplied by the average number of encoder pulses (N_e) from the two encoders. For a typical NIST calibration the piston stroke for each calibration point uses 85 % of the total cylinder length (or 85 % of the total cylinder volume) for flows ranging from 151 lpm down to 5.7 lpm. As shown in Table 2 the length of the piston stroke decreases at lower flows so that the stroke duration is $\Delta t_{max} = 120$ s. The two shafts on either side of the piston both have nominal diameters of $d = 2.54$ cm, while the nominal cylinder diameter is $D = 15.24$ cm. Moreover, both d and D are machined so that cross sectional area $A_{cs} = \pi (D^2 \text{-} d^2)/4$ can be taken as a constant along the cylinder length.

Table 2. *Typical values for the length of the piston stroke, duration of the piston stroke, number of encoder pulses during the piston stroke, percent of cylinder volume used relative to the total volume for a typical calibration point.*

Flow at Cylinder (Q_{cyl})		Piston Velocity	Duration of Piston Stroke (Δt)	Length of Piston Stroke	Encoder Pulses (N_e)	Percent of Cylinder Volume Used
[lpm]	[gal]	[cm/s]	[s]	[cm]	[pulse]	[%]
151.3	40	14.2	5	64.8	32385	85
113.4	30	10.7	6	64.8	32385	85
75.7	20	7.1	9	64.8	32385	85
37.8	10	3.5	18	64.8	32385	85
19.0	5	1.8	36	64.8	32385	85
3.8	1	0.4	120	42.6	21286	56
1.1	0.3	0.1	120	12.6	6301	17

2.2. Flow Measurement Principle

Flow determinations are based on the piston displacing a known volume of fluid over a measured time interval. The volumetric flow exiting the cylinder is

$$Q_{cyl} = \frac{K_V N_e}{\Delta t} \tag{1}$$

where K_V is the calibrator constant or herein called the *volumetric prover K-factor* with units of volume per encoder pulse. This geometric parameter equals[c]

$$K_V = A_{cs} \Delta L'_e \tag{2}$$

the cross sectional area multiplied by the encoder constant, and is nearly constant except for a slight dependence on the fluid operating temperature and pressure and on the room temperature. At different operating conditions thermal expansion and pressure loading change the cylinder and shaft diameters, and consequently A_{cs}. Similarly, thermal expansion causes $\Delta L'_e$ to change with the room temperature conditions. Instead of charactering K_V over the range of prover operating conditions, standard practice is to determine its value at a single reference temperature (T_{ref}) and pressure (P_{ref}), and correct volumetric flow calculations for *reference condition effects* using

$$D = D_{ref}[1 + \alpha_{st}(T - T_{ref})], \tag{3a}$$

$$d = d_{ref}[1 + \alpha_{st}(T - T_{ref})], \tag{3b}$$

$$\Delta L'_e = \Delta L'_{e,ref}[1 + \alpha_{en}(T_{en} - T_{ref})] \tag{3c}$$

where $\alpha_{st} = 1.7 \times 10^{-5} \text{ K}^{-1}$ and $\alpha_{en} = 8 \times 10^{-6} \text{ K}^{-1}$ are the linear expansion coefficients for the stainless steel shafts and cylinder and for the glass encoder scale, and T_{en} and T are the

---

[c] The diameters of the shafts on either side of the piston are slightly different so that the cross sectional area differs slightly when the piston sweeps to the left verses to the right. To accommodate this difference it is common practice to distinguish the value of the volumetric prover K-factor when the piston sweeps left ($K_{V,left}$) from when the piston sweeps right ($K_{V,right}$).

temperatures of the encoder and the fluid.[d] Elastic deformation caused by pressure stresses can be neglected since the cylinder cross sectional area changes by less 0.004% at the maximum operating pressure. To minimize the uncertainties introduced by the linear temperature approximation used in Eq. (3), the prover operating conditions should be maintained close to T_{ref} and P_{ref}. In this way, the theoretically corrected reference condition effects are small relative to the measured $K_{\text{v}}^{\text{ref}}$ values.

The three commonly used methods to determine the reference volumetric prover K-factor ($K_{\text{v}}^{\text{ref}}$) are 1) a water draw procedure [4], 2) dimensional measurements of the cylinder diameter (D_{ref}), the shaft diameters on either side of the piston (d_{ref}), and the encoder constant ($\Delta L'_{\text{e,ref}}$) [1], and 3) use of a transfer standard flowmeter [4]. In this work $K_{\text{v}}^{\text{ref}}$ is determined using the water draw method explained in section 4.1.

2.3. Flow at the MUT under *Ideal* Conditions

When the prover is operated at the reference conditions the volumetric flow exiting the cylinder is $Q_{\text{cyl}}^{\text{ref}} = K_{\text{v}}^{\text{ref}} N_{\text{e}}/\Delta t$, and the mass flow is $\dot{m}_{\text{cyl}}^{\text{ref}} = \rho_{\text{ref}} K_{\text{v}}^{\text{ref}} N_{\text{e}}/\Delta t$ where ρ_{ref} is the fluid density evaluated at P_{ref} and T_{ref}. The objective of a piston prover standard is to determine the flow at the MUT using theses reference flows. However, the volumetric and mass flow at the MUT only equal the respective reference flows (*i.e.*, $Q_{\text{MUT}}^{\text{ideal}} = Q_{\text{cyl}}^{\text{ref}}$ and $\dot{m}_{\text{MUT}}^{\text{ideal}} = \dot{m}_{\text{cyl}}^{\text{ref}}$) under the following idealized conditions

1) steady flow,
2) room temperature equal to T_{ref},
3) fluid temperature equal to T_{ref} throughout the cylinder and test section,
4) fluid pressure equals P_{ref} throughout the cylinder and test section, and
5) no leaks into or out of the piston-cylinder and test section.

NIST operates its 20 L HLFS as close as possible to these idealized conditions. Steady flow conditions are obtained by stroking the piston at a nearly constant velocity during data collection. The fluid temperature is controlled to T_{ref} using the heat exchanger shown in Fig. 1. Temperature uniformity of the fluid in the prover assembly is established by cycling the piston back and forth until the 5 temperature sensors distributed throughout the test section and the 2 temperature sensors located at the left and right exits of the piston-cylinder assembly agree to within 0.5 C or better. The room housing the 20 L HLFS is maintained to within ± 3 °C of the reference temperature to minimize heat transfer effects. The fluid pressure is maintained slightly above P_{ref} (*i.e.*, between 150 kPa and 315 kPa) to prevent measurement errors and possible damage caused by cavitation to customer turbine meters.

Leaks from the 20 L HLFS can be either external (*i.e.*, leakage from the prover to the room) or internal (*i.e.*, leakage past the four-way valve or past the piston). External leaks are visible and easily fixed. Internal leaks past the piston are prevented using two hydraulic wiper seals, one on either side of the piston. If either seal fails, the piston interior is designed with apertures that allow the leak to drain into the hollow piston shaft until it becomes visible at the opposite end of the shaft when it drips onto the floor. Leakage past the four-way valve is identified indirectly by monitoring the

---

[d] The fluid temperature is assumed to be in thermal equilibrium with the cylinder and shaft, and the encoder temperature is assumed equal to the room temperature.

consistency of the check standard permanently installed in the test section. In this way, errors attributed to leaks can be minimized and are herein taken to be zero.

2.4. Corrections for Non-Ideal Operating Conditions

The ideal flow conditions listed in section 2.3 are never perfectly realized in practice. To improve flow measurement accuracy corrections are made to Q_{MUT}^{ideal} and $\dot{m}_{MUT}^{ideal}$ to account for small deviations from ideal conditions. In particular, corrections are made to account for non-idealities caused 1) by *reference condition effects* and 2) by *gradient effects* (*i.e.*, spatial non-uniformities in the temperature and/or pressure distribution). Corrections for reference condition effects are made when the operating conditions (*i.e.*, fluid temperature, fluid pressure, and room temperature differ from T_{ref} and P_{ref}. These corrections account either for changes in the cylinder volume (as already discussed in section 2.2) or for changes in the fluid density. Reference condition corrections for changes in the fluid density are calculated using a linear function of temperature and pressure

$$\rho = \rho_{ref}\left[1 - \beta(T - T_{ref}) + \kappa(P - P_{ref})\right] \tag{4}$$

where β is the thermal expansion coefficient and κ is the isothermal compressibility factor (or the inverse of the isothermal bulk modulus).

Pressure and temperature differences between the fluid exiting the cylinder and the fluid at the MUT cause the volumetric flow at these two locations to differ. These *gradient effects* are caused by pressure loss mechanisms such as wall friction, elbows, fittings, etc., as well as by heat transfer caused by temperature differences between the fluid and the room. Gradient effects are corrected by measuring the temperature and pressure at the cylinder exit and at the MUT. The measured temperatures and pressures are used in Eq. 3 to calculate the density at the cylinder exit (ρ_{cyl}) and at the MUT (ρ_{MUT}). Based on mass conservation, the volumetric flow at the MUT is taken to be equal to the volumetric flow at the MUT multiplied by the density ratio (ρ_{cyl}/ρ_{MUT}).

A third type of non-ideality results from an unsteady flow. In this case the mass flow exiting the cylinder is not equal to the mass flow at the MUT. The difference in mass flows is attributed to mass accumulation in the volume of piping that connects the prover to the MUT. That is, the mass in this volume at the start of the piston stroke is not equal to mass at the end of the piston stroke. NIST does not currently correct for *mass storage effects*. However, for each calibration we estimate the magnitude of these effects and include them in the uncertainty budget.

3. Formulation of Governing Flow Equations

(a) Prover at $t = t^i$

(b) Prover at $t = t^f$
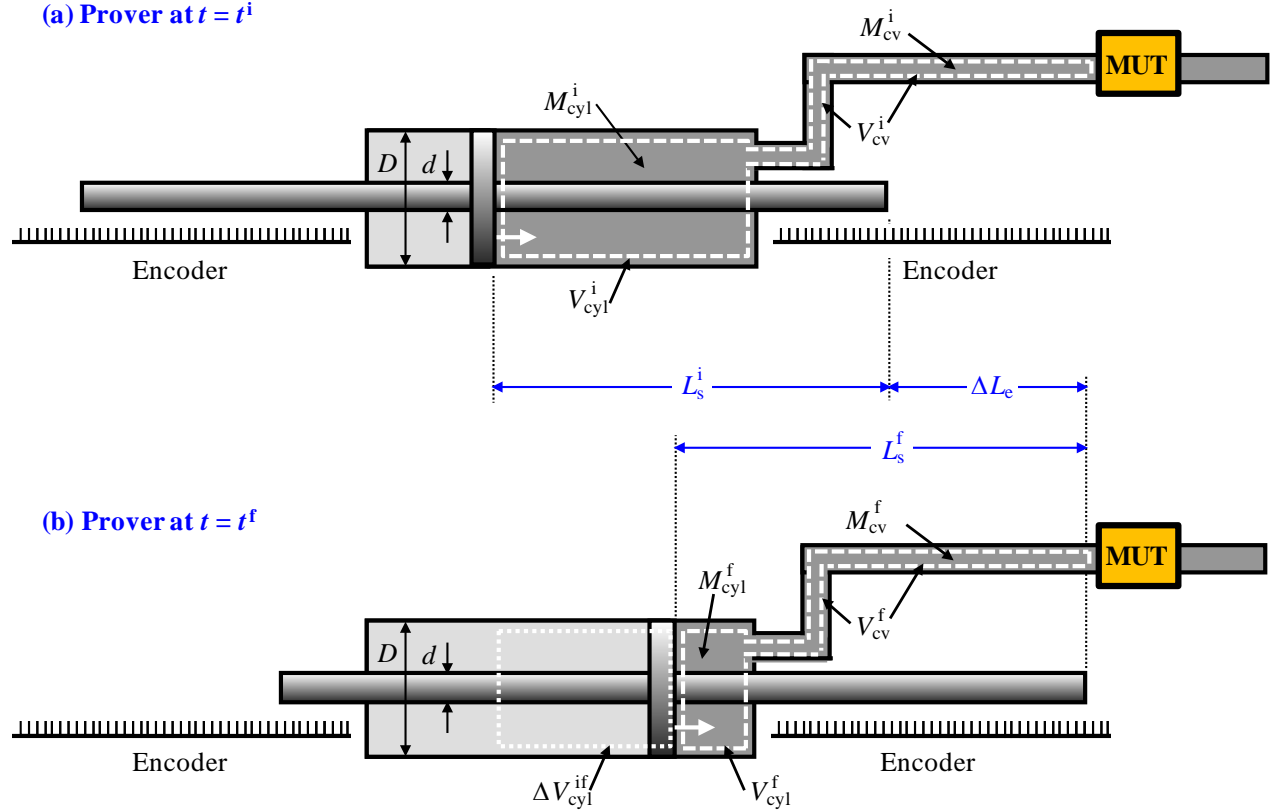
Figure 3. *Sketch showing the orientation of the piston before and after the piston stroke.*

Figures 3a and 3b show the location of the piston at the start of the measured time interval (t_i) and at the end of the measured time interval (t_f). The white dashed lines constitute the *control volume* where mass conservation is applied. The control volume includes the volume of fluid to the right of the piston inside the cylinder (V_{cyl}), and the fluid in the connecting volume between the exit of the cylinder and the MUT (V_{cv}). As the piston strokes rightward the size of the control volume decreases such that the time-averaged mass flow through the MUT is

$$\tilde{m}_{MUT} = \frac{\Delta M_{cyl}^{if}}{\Delta t} + \frac{\Delta M_{cv}^{if}}{\Delta t} - \tilde{m}_{leak} \tag{5}$$

where $\Delta M_{cyl}^{if} = M_{cyl}^i - M_{cyl}^f$ is difference between the initial and final mass in the cylinder, $\Delta M_{cv}^{if} = M_{cv}^i - M_{cv}^f$ is difference between the initial and final mass in the connecting volume, $\Delta t = t_f - t_i$ is the measured time interval, and $\tilde{m}_{leak}$ is net time-averaged mass flow leaking out of the control volume. Alternatively, the mass terms in Eq. (5) can be expressed

$$\tilde{m}_{MUT} = \frac{\hat{\rho}_{cyl}^i V_{cyl}^i - \hat{\rho}_{cyl}^f V_{cyl}^f}{\Delta t} + \frac{\hat{\rho}_{cv}^i V_{cv}^i - \hat{\rho}_{cv}^f V_{cv}^f}{\Delta t} - \tilde{m}_{leak}$$

or

$$\tilde{m}_{MUT} = \left[\frac{\hat{\rho}^i V^i - \hat{\rho}^f V^f}{\Delta t} \right]_{cyl} + \left[\frac{\hat{\rho}^i V^i - \hat{\rho}^f V^f}{\Delta t} \right]_{cv} - \tilde{m}_{leak} \tag{6}$$

as density multiplied by volume (*e.g.*, $M_{\text{cyl}}^{\text{i}} = \hat{\rho}_{\text{cyl}}^{\text{i}} V_{\text{cyl}}^{\text{i}}$, $M_{\text{cv}}^{\text{i}} = \hat{\rho}_{\text{cv}}^{\text{i}} V_{\text{cv}}^{\text{i}}$).[e] By adding and subtracting the terms $\hat{\rho}_{\text{cyl}}^{\text{i}} V_{\text{cyl}}^{\text{f}}$ and $\hat{\rho}_{\text{cv}}^{\text{i}} V_{\text{cv}}^{\text{f}}$ to the right side of Eq. (6) the time-averaged mass flow (with no leaks) is

$$\tilde{m}_{\text{M U}} = \left[\frac{\hat{\rho}^{\text{i}} V^{\text{i}} - \hat{\rho}^{\text{f}} V^{\text{f}} + \left(\hat{\rho}^{\text{i}} V^{\text{f}} - \hat{\rho}^{\text{i}} V^{\text{f}}\right)}{\Delta t}\right]_{\text{cyl}} + \left[\frac{\hat{\rho}^{\text{i}} V^{\text{i}} - \hat{\rho}^{\text{f}} V^{\text{f}} + \left(\hat{\rho}^{\text{i}} V^{\text{f}} - \hat{\rho}^{\text{i}} V^{\text{f}}\right)}{\Delta t}\right]_{\text{cv}}$$

$$= \left[\frac{\left(\hat{\rho}^{\text{i}} V^{\text{i}} - \hat{\rho}^{\text{i}} V^{\text{f}}\right) + \left(\hat{\rho}^{\text{i}} V^{\text{f}} - \hat{\rho}^{\text{f}} V^{\text{f}}\right)}{\Delta t}\right]_{\text{cyl}} + \left[\frac{\left(\hat{\rho}^{\text{i}} V^{\text{i}} - \hat{\rho}^{\text{i}} V^{\text{f}}\right) + \left(\hat{\rho}^{\text{i}} V^{\text{f}} - \hat{\rho}^{\text{f}} V^{\text{f}}\right)}{\Delta t}\right]_{\text{cv}}$$

$$= \left[\frac{\hat{\rho}^{\text{i}} \Delta V^{\text{if}} + \Delta\hat{\rho}^{\text{if}} V^{\text{f}}}{\Delta t}\right]_{\text{cyl}} + \left[\frac{\hat{\rho}^{\text{i}} \Delta V^{\text{if}} + \Delta\hat{\rho}^{\text{if}} V^{\text{f}}}{\Delta t}\right]_{\text{cv}}$$

$$= \frac{\hat{\rho}_{\text{cyl}}^{\text{i}} \Delta V_{\text{cyl}}^{\text{if}}}{\Delta t} + \frac{V_{\text{cyl}}^{\text{f}} \Delta\hat{\rho}_{\text{cyl}}^{\text{if}}}{\Delta t} + \frac{\hat{\rho}_{\text{cv}}^{\text{i}} \Delta V_{\text{cv}}^{\text{if}}}{\Delta t} + \frac{V_{\text{cv}}^{\text{f}} \Delta\hat{\rho}_{\text{cv}}^{\text{if}}}{\Delta t}$$

$$\tilde{m}_{\text{M U}} = \left(\frac{\hat{\rho}_{\text{cyl}}^{\text{i}} \Delta V_{\text{cyl}}^{\text{if}}}{\Delta t}\right)\left[1 + \frac{V_{\text{cyl}}^{\text{f}}}{\Delta V_{\text{cyl}}^{\text{if}}} \frac{\Delta\hat{\rho}_{\text{cyl}}^{\text{if}}}{\hat{\rho}_{\text{cyl}}^{\text{i}}} + \frac{V_{\text{cv}}^{\text{f}}}{\Delta V_{\text{cyl}}^{\text{if}}} \frac{\Delta\hat{\rho}_{\text{cv}}^{\text{if}}}{\hat{\rho}_{\text{cyl}}^{\text{i}}} + \frac{\hat{\rho}_{\text{cv}}^{\text{i}}}{\hat{\rho}_{\text{cyl}}^{\text{i}}} \frac{\Delta V_{\text{cv}}^{\text{if}}}{\Delta V_{\text{cyl}}^{\text{if}}}\right] \tag{7}$$

where $\Delta V_{\text{cyl}}^{\text{if}} = V_{\text{cyl}}^{\text{i}} - V_{\text{cyl}}^{\text{f}}$ is the volume swept by the piston during the measurement interval indicated by the dotted lines in Fig. 2b. The terms in the square brackets account for mass storage in the portion of the cylinder volume not swept by the piston ($V_{\text{cyl}}^{\text{f}}$) shown in Fig. 2b, and in the connecting volume (V_{cv}). Here, $\Delta\hat{\rho}_{\text{cyl}}^{\text{if}} = \hat{\rho}_{\text{cyl}}^{\text{i}} - \hat{\rho}_{\text{cyl}}^{\text{f}}$ and $\Delta\hat{\rho}_{\text{cv}}^{\text{if}} = \hat{\rho}_{\text{cv}}^{\text{i}} - \hat{\rho}_{\text{cv}}^{\text{f}}$ are the density differences in the unswept cylinder volume and in the connecting piping between the start and stop of a flow measurement. Similarly, $\Delta V_{\text{cv}}^{\text{if}} = V_{\text{cv}}^{\text{i}} - V_{\text{cv}}^{\text{f}}$ is the change in the connecting volume between the start and stop of a flow measurement.

The time-averaged volumetric flow at the MUT is determined by dividing Eq. (7) by the time-averaged density at the MUT ($\tilde{\rho}_{\text{MUT}}$)

$$\tilde{Q}_{\text{MUT}} = \left(\frac{\Delta V_{\text{cyl}}^{\text{if}}}{\Delta t}\right)\left[\frac{\hat{\rho}_{\text{cyl}}^{\text{i}}}{\tilde{\rho}_{\text{MUT}}} + \frac{V_{\text{cyl}}^{\text{f}}}{\Delta V_{\text{cyl}}^{\text{if}}} \frac{\Delta\hat{\rho}_{\text{cyl}}^{\text{if}}}{\tilde{\rho}_{\text{MUT}}} + \frac{V_{\text{cv}}^{\text{f}}}{\Delta V_{\text{cyl}}^{\text{if}}} \frac{\Delta\hat{\rho}_{\text{cv}}^{\text{if}}}{\tilde{\rho}_{\text{MUT}}} + \frac{\hat{\rho}_{\text{cv}}^{\text{i}}}{\tilde{\rho}_{\text{MUT}}} \frac{\Delta V_{\text{cv}}^{\text{if}}}{\Delta V_{\text{cyl}}^{\text{if}}}\right] - \frac{\tilde{m}_{\text{leak}}}{\tilde{\rho}_{\text{MUT}}}. \tag{8}$$

As expected, both Eq. 7 and 8 simplify to $\dot{m}_{\text{MUT}}^{\text{ideal}} = \dot{m}_{\text{cyl}}^{\text{ref}}$ and $Q_{\text{MUT}}^{\text{ideal}} = Q_{\text{cyl}}^{\text{ref}}$ for the ideal operating conditions given in section 2.2.

3.1 Mass Flow and Volumetric Flow at the MUT

Equations 7 and 8 for the MUT mass flow and volumetric flow can be compactly expressed by

---

[e] Note that $\hat{\rho}$ is the spatially averaged density.

$$\tilde{m}_{\text{MUT}} = \left(\frac{\rho_{\text{ref}} K_V^{\text{ref}} N_e}{\Delta t} \right) R_1 R_2 R_3 R_4 R_5 S_1 S_2 S_3 S_4 S_5 S_6 \tag{9a}$$

and

$$\tilde{Q}_{\text{MUT}} = \left[\frac{K_V^{\text{ref}} N_e}{\Delta t} \right] R_1 R_2 R_3 S_1 S_2 S_3 \, S_4 S_5 S_6 G_1 G_2 \tag{9b}$$

where the near unity correction factors indicated by the R_i's, G_i's, and S_i's account for *reference condition corrections*, *gradient corrections*, and *storage corrections*, respectively. The R_i's, correct the fluid density and the measured cylinder volume to the reference conditions. The G_i's correct the flow when pressures and temperatures gradients exist between the piston-cylinder assembly and the MUT. The S_i's are mass *storage* corrections to account for differences in the cylinder and in the connecting volume between the start and stop of a flow measurement. Expressions for these correction factors are given in Table 3 along with a description of their physical meaning.

Many of the correction factors listed in Table 3 are essentially unity for the NIST operating conditions and do not affect flow calculations. Nevertheless, these correction factors have been retained to provide guidance for applications when operating conditions cannot be maintained close to the reference conditions. However, we point out that potential mechanical problems such as seal failure should also be considered for extreme operating conditions. For clarity, we specify correction factors that can be neglected when using Eq. (9a) and (9b) in the remaining sections of the manuscript.

The S_i's correction factors in Table 3 show the need to measure temperature and pressure at t_i and at t_f to correct for storage effects. Moreover, the time response of the pressure and temperature instrumentation should be sufficiently fast to resolve transients. Although NIST intends to upgrade its software and instrumentation to enable reliable storage corrections in the future, the prover is not currently equip to make these measurements. Instead, we use Table 3 to estimate the size of storage corrections. For NIST operating conditions S_3 is by far the most significant correction factor. Its value is estimated by monitoring how the prover temperature changes during the repeated data points of a calibration. Typically, the temperature change is less than 100 mK so that $S_3 < 0.01$ %.

Table 3. *Correction factors for mass flow in Eq. (9a) and volumetric flow in Eq. (9b).*

Region of Prover where Correction Applies	Equation	Type of Correction	Description
Encoder	$R_1 = 1 + \alpha_{\text{en}}\left(T_{\text{en}} - T_{\text{ref}}\right)$	*Reference* Condition Correction	Axial change of encoder scale from the *reference* condition due to thermal expansion
Displaced Volume	$R_2 = 1 + 2\,\alpha_{\text{st}}\left(\hat{T}_{\text{cyl}}^{\text{i}} - T_{\text{ref}}\right)$	*Reference* Condition Correction	Radial change in the cylinder and shaft from *reference* condition due to thermal expansion
Displaced Volume	$R_3 = 1 + 2\,\varepsilon_{\text{eff}}\left(\hat{P}_{\text{cyl}}^{\text{i}} - P_{\text{ref}}\right)$	*Reference* Condition Correction	Radial change in cylinder and shaft from the *reference* condition due to internal fluid pressure[f]
Displaced Volume	$R_4 = 1 - \beta\left(\hat{T}_{\text{cyl}}^{\text{i}} - T_{\text{ref}}\right)$	*Reference* Condition Correction	Change in the fluid density from the *reference* density (ρ_{ref}) due to thermal expansion
Displaced Volume	$R_5 = 1 + \kappa\left(\hat{P}_{\text{cyl}}^{\text{i}} - P_{\text{ref}}\right)$	*Reference* Condition Correction	Change in the fluid density from the *reference* density (ρ_{ref}) due to pressure change from P_{ref}
Displaced Volume/MUT	$G_1 = 1 - \beta\left(\hat{T}_{\text{cyl}}^{\text{i}} - \tilde{T}_{\text{MUT}}\right)$	Temperature *Gradient* Correction	Ratio density change between cylinder and MUT attributed to temperature difference between the cylinder and MUT
Displaced Volume/MUT	$G_2 = 1 + \kappa\left(\hat{P}_{\text{cyl}}^{\text{i}} - \tilde{P}_{\text{MUT}}\right)$	Pressure *Gradient* Correction	Ratio density change between cylinder and MUT attributed to pressure difference between the cylinder and MUT
Upswept Volume of Cylinder	$S_1 = 1 + 2\left(\dfrac{V_{\text{cyl}}^{\text{f}}}{N_{\text{e}}K_{\text{V}}^{\text{ref}}}\right)\alpha_{\text{st}}\left(\hat{T}_{\text{cyl}}^{\text{i}} - \hat{T}_{\text{cyl}}^{\text{f}}\right)$	Mass *Storage*	Radial change in the unswept region of the cylinder and shaft diameters due to a temperature change between the start and stop of a calibration
Upswept Volume of Cylinder	$S_2 = 1 + 2\left(\dfrac{V_{\text{cyl}}^{\text{f}}}{N_{\text{e}}K_{\text{V}}^{\text{ref}}}\right)\varepsilon_{\text{eff}}\left(\hat{P}_{\text{cyl}}^{\text{i}} - \hat{P}_{\text{cyl}}^{\text{f}}\right)$	Mass *Storage*	Radial change in the unswept region of the cylinder and shaft diameters due to a pressure change between the start and stop of a calibration
Upswept Volume of Cylinder	$S_3 = 1 - \left(\dfrac{V_{\text{cyl}}^{\text{f}}}{N_{\text{e}}K_{\text{V}}^{\text{ref}}}\right)\beta\left(\hat{T}_{\text{cyl}}^{\text{i}} - \hat{T}_{\text{cyl}}^{\text{f}}\right)$	Mass *Storage*	Change in the fluid density in the unswept region of the cylinder due to a temperature change between the start and stop of a calibration
Upswept Volume of Cylinder	$S_4 = 1 + \left(\dfrac{V_{\text{cyl}}^{\text{f}}}{N_{\text{e}}K_{\text{V}}^{\text{ref}}}\right)\kappa\left(\hat{P}_{\text{cyl}}^{\text{i}} - \hat{P}_{\text{cyl}}^{\text{f}}\right)$	Mass *Storage*	Change in the fluid density in the unswept region of the cylinder due to a pressure change between the start and stop of a calibration
Connecting Volume	$S_5 = 1 + \left(\dfrac{V_{\text{cv}}^{\text{ref}}}{N_{\text{e}}K_{\text{V}}^{\text{ref}}}\right)\left(3\alpha_{\text{cv}} - \beta\right)\left(\hat{T}_{\text{cyl}}^{\text{i}} - \hat{T}_{\text{cyl}}^{\text{f}}\right)$	Mass *Storage*	Change in the connecting volume and the density of fluid in this region due to a temperature change between the start and stop of a calibration[g]
Connecting Volume	$S_6 = 1 + \left(\dfrac{V_{\text{cv}}^{\text{ref}}}{N_{\text{e}}K_{\text{V}}^{\text{ref}}}\right)\left(2\varepsilon_{\text{cv}} + \kappa\right)\left(\hat{P}_{\text{cyl}}^{\text{i}} - \hat{P}_{\text{cyl}}^{\text{f}}\right)$	Mass *Storage*	Mass storage in connecting volume attributed to pressure difference between start and stop of flow measurement

[f] Note that ε_{eff} and ε_{cv} are parameters with units of inverse pressure to be determined using the appropriate pressure vessel equations in terms of the material modulus of elasticity, Poisson ratio, and dimensions.

[g] Note that α_{cv} is the linear coefficient of expansion for the connecting volume material.

5. Uncertainty Analysis

The method of propagation of uncertainty [5] as specified in the GUM [6] is used to determine the uncertainties of the volumetric prover K-factor determined by the water draw procedure, the volumetric flow at the MUT, and the mass flow at the MUT. For each of these quantities the relevant uncertainty sources are taken to be uncorrelated. Standard uncertainties (*i.e.*, 68 % confidence level) are multiplied by their sensitivity coefficients and root-sum-squared (RSS) to determine the expanded uncertainties (or approximate 95 % confidence level).

5.1 Determined and Uncertainty the Volumetric Prover K-factor (K_V^{ref})

The reference volumetric prover K-factor (K_V^{ref}) is determined using a water draw procedure at a reference temperature and pressure of $T_{\text{ref}} = 21\,ºC$ and $P_{\text{ref}} = 101.325$ kPa. After temperature equilibrium is established in the both the room and the fluid, the piston is slowly traverse through the cylinder and the displaced fluid is directed into a weigh tank instead of through the MUT. Thus, we determine K_V^{ref} using Eq. (9a) for mass flow. However, the total mass that would have passed through the MUT (*i.e.*, $\tilde{m}_{\text{MUT}}\,\Delta t$) is replaced by the buoyancy corrected and calibrated weigh scale readings as shown in

$$K_V^{\text{ref}} = \frac{\left(M_T^f - M_T^i\right)\left(1 - \rho_{\text{air}}/\rho_{\text{ref}}\right)^{-1}}{N_e \rho_{\text{ref}}\left(\prod_{n=1}^{5} R_n\right)\left(\prod_{n=1}^{7} S_n\right)}$$

or

$$K_V^{\text{ref}} = \frac{\left(M_T^f - M_T^i\right)\left(1 - \rho_{\text{air}}/\rho_{\text{ref}}\right)^{-1}}{N_e \rho_{\text{ref}}[1 - \beta(\hat{T}_{\text{cyl}}^i - T_{\text{ref}})]}$$

(10)

where M_T^i is the tare weight of the empty collection vessel (after zeroing the scale), and M_T^f is the final scale reading after the filling the collection vessel, and the quantity $(1 - \rho_{\text{air}}/\rho_{\text{ref}})^{-1}$ is the buoyancy correction. The air density (ρ_{air}) is calculated as a function of the pressure, temperature, and relative humidity in the room using the correlation developed by Jaeger and Davis. [7] During the K_V^{ref} measurement the room temperature was controlled to within $\pm 2°C$ of T_{ref}, the fluid temperature was controlled to within $\pm 0.1°C$ of T_{ref}, and the fluid pressure was 100 kPa $\pm 1.5°$kPa. For these conditions $R_4 = 1 - \beta(\hat{T}_{\text{cyl}}^i - T_{\text{ref}})$ is the only significant correction factor as shown in Eq. (6). All of the other reference condition and storage corrections attribute less than 0.004 % to K_V^{ref} and are neglected.

The volumetric prover K-factor was measured on two occasions, first on April 2008, and a second time on Jan 2009. Measurements were done with the piston stroking to the left ($K_{V,\text{left}}^{\text{ref}}$) and then with the piston stroking right ($K_{V,\text{right}}^{\text{ref}}$). On the first occasion $K_{V,\text{left}}^{\text{ref}}$ and $K_{V,\text{right}}^{\text{ref}}$ were measured 20 times each using Stoddard solvent as the working fluid. On the second occasion $K_{V,\text{left}}^{\text{ref}}$ was measured 5 times while $K_{V,\text{right}}^{\text{ref}}$ was measured 8 times using reverse osmosis water as the working fluid. As seen

in Fig. 4 the difference between $K_{V,left}^{ref}$ and $K_{V,right}^{ref}$ is less than 0.01 % for the measurements in Stoddard solvent and the measurements in water. Based on this good agreement the average volumetric K-factor can be used for both directions without significant increase in the uncertainty, $K_V^{ref} = (K_{V,left}^{ref} + K_{V,left}^{ref})/2$.
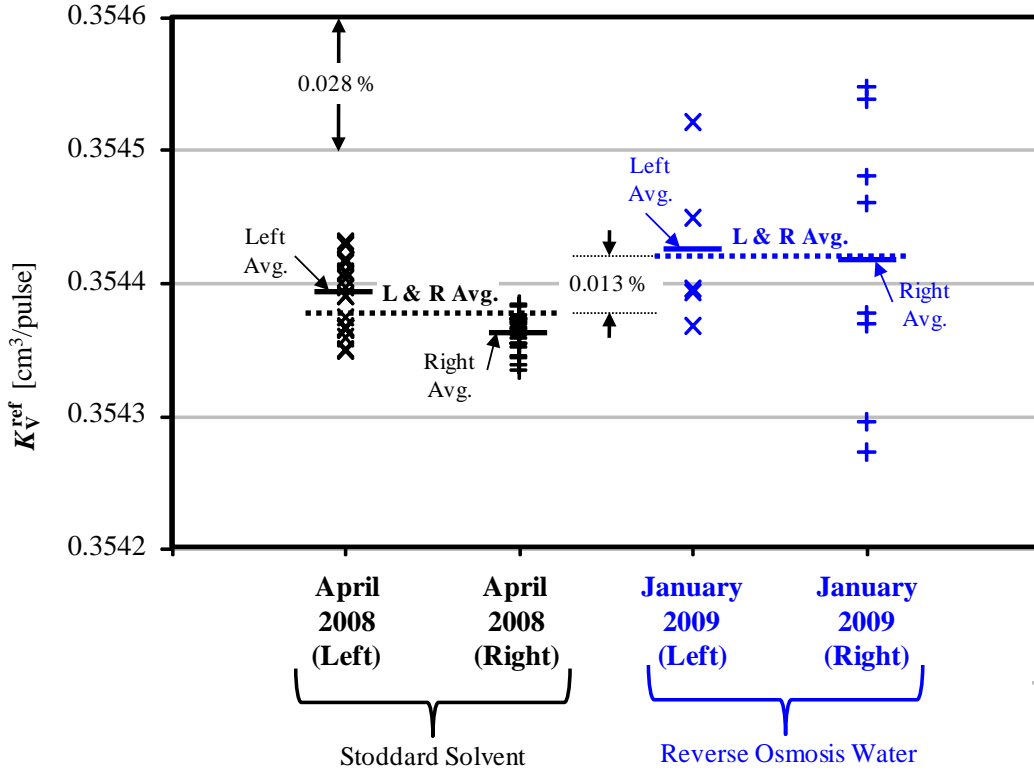
Figure 4. *Plot showing measurements of the volumetric prover K-factor done in April 2008 in Stoddard solvent and on January 2009 in reverse osmosis water.*

The data measured collected in January 2009 was substantially noisier than the data taken on April 2008, possibly due to a small leak from the four-way valve. However, the difference between the average K-factors obtained from April 2008 and from January 2009 is only 0.013 %. The expression used to calculate the uncertainty of the measured K-factor is given by Eq. (11)

$$\left[\frac{u(K_V^{ref})}{K_V^{ref}}\right]^2 = \left[\frac{M_s^i}{K_V^{ref}}\frac{\partial K_V^{ref}}{\partial M_s^i}\right]^2\left[\frac{u(M_s^i)}{M_s^i}\right]^2 + \left[\frac{M_s^f}{K_V^{ref}}\frac{\partial K_V^{ref}}{\partial M_s^f}\right]^2\left[\frac{u(M_s^f)}{M_s^f}\right]^2 + \left[\frac{\beta}{K_V^{ref}}\frac{\partial K_V^{ref}}{\partial \beta}\right]^2$$

$$+ \left[\frac{\rho_{ref}}{K_V^{ref}}\frac{\partial K_V^{ref}}{\partial \rho_{ref}}\right]^2\left[\frac{u(\rho_{ref})}{\rho_{ref}}\right]^2 + \left[\frac{\rho_{air}}{K_V^{ref}}\frac{\partial K_V^{ref}}{\partial \rho_{air}}\right]^2\left[\frac{u(\rho_{air})}{\rho_{air}}\right]^2 + \left[\frac{u(N_e)}{N_e}\right]^2 \quad (11)$$

$$+ \left[\frac{\hat{T}_{cyl}^i}{K_V^{ref}}\frac{\partial K_V^{ref}}{\partial \hat{T}_{cyl}^i}\right]^2\left[\frac{u(\hat{T}_{cyl}^i)}{\hat{T}_{cyl}^i}\right]^2 + \frac{\sigma_{left}^2}{N} + \frac{\sigma_{right}^2}{N} + \left|\frac{K_{V,left}^{ref} - K_{V,right}^{ref}}{K_{V,right}^{ref}\sqrt{3}}\right|^2$$

where σ_{left} and σ_{right} are the standard deviations of the repeated measurements for the piston stroking in the leftward and rightward. Table 4 itemizes the each uncertainty component.

Table 4. *Uncertainty budget for volumetric prover K-factor corresponding to Eq. (10).*

Vol. Prover K-factor $K_V^{ref} = 0.35437$ [cm³/pulse]	Nom. Value [SI]	Rel. Unc. (k=1) [%]	Norm. Sen. Coeff. [ ]	Type A/B [ ]	Perc. Contrib. [%]	Comments
Initial Scale Mass, $M_{T,i}$ [kg]	0	0.0118	0.0017	B	0	Control Charts of 60 kg scale
Final Scale Mass, $M_{s,f}$ [kg]	13.4017	0.0118	0.9983	B	10.2	Control Charts of 60 kg scale
Water Density, ρ_{ref} [kg/m³]	99702	0.002	-1.002	B	0.3	Density of Reverse Osmosis Water[8]
Air Density, ρ_{air} [kg/m³]	1.162	2	0.0015	B	0.7	Air Density [7] and measured T, P, and RH
Encoder Pules, N_e [pulse]	37606	0	-1	B	0.2	Integer number of pulses
Thermal Expan. Coeff., β [1/°C]	-0.00097	10	0.0001	B	0.1	Anton Paar Density Meas. Fit Residuals
Intial Fluid Temp., Tf_i [°C]	21.14	0.017	0.27	B	1.7	Cal. Records and spatial non-uniformity of 6 thermistors
Repeat. of 5 meas. (left)	N/A	0.017	1	A	22.2	Stdev. of the mean of 5 meas.
Repeat. of 8 meas. (right)	N/A	0.0296	1	A	64.6	Stdev. of the mean of 8 meas.
Diff betwn. left and right	N/A	0.001	1	B	0	Rect. Dist. Assumed
RSS		**0.037**			**100**	

5.2 Uncertainty of the Volumetric and Mass Flow at the MUT

The volumetric flow at the MUT is determined using Eq.(9b). The expression used to calculate the uncertainty of the MUT is Eq. (11) and Table 5 itemizes the uncertainty of each component.

$$
\left[\frac{u(\tilde{Q}_{MUT})}{\tilde{Q}_{MUT}}\right]^2 = \left[\frac{u(K_V^{ref})}{K_V^{ref}}\right]^2 + \left[\frac{u(N_e)}{N_e}\right]^2 + \left[\frac{u(\Delta t)}{\Delta t}\right]^2 + \left(\frac{\tilde{T}_{MUT}}{\tilde{Q}_{MUT}}\frac{\partial \tilde{Q}_{MUT}}{\partial \tilde{T}_{MUT}}\right)^2\left[\frac{u(\tilde{T}_{MUT})}{\tilde{T}_{MUT}}\right]^2
$$

$$
+ \left(\frac{T_{en}}{\tilde{Q}_{MUT}}\frac{\partial \tilde{Q}_{MUT}}{\partial T_{en}}\right)^2\left[\frac{u(T_{en})}{T_{en}}\right]^2 + \left(\frac{\hat{T}_{cyl}^i}{\tilde{Q}_{MUT}}\frac{\partial \tilde{Q}_{MUT}}{\partial \hat{T}_{cyl}^i}\right)^2\left[\frac{u(\hat{T}_{cyl}^i)}{\hat{T}_{cyl}^i}\right]^2
$$

$$
+ \left(\frac{\hat{P}_{cyl}^i}{\tilde{Q}_{MUT}}\frac{\partial \tilde{Q}_{MUT}}{\partial \hat{P}_{cyl}^i}\right)^2\left[\frac{u(\hat{P}_{cyl}^i)}{\hat{P}_{cyl}^i}\right]^2 + \left(\frac{\tilde{P}_{MUT}}{\tilde{Q}_{MUT}}\frac{\partial \tilde{Q}_{MUT}}{\partial \tilde{P}_{MUT}}\right)^2\left[\frac{u(\tilde{P}_{MUT})}{\tilde{P}_{MUT}}\right]^2
$$

$$
+ \left(\frac{\beta}{\tilde{Q}_{MUT}}\frac{\partial \tilde{Q}_{MUT}}{\partial \beta}\right)^2\left[\frac{u(\beta)}{\beta}\right]^2 + \left(\frac{\alpha_{en}}{\tilde{Q}_{MUT}}\frac{\partial \tilde{Q}_{MUT}}{\partial \alpha_{en}}\right)^2\left[\frac{u(\alpha_{en})}{\alpha_{en}}\right]^2
$$

$$
+ \left(\frac{\alpha_{st}}{\tilde{Q}_{MUT}}\frac{\partial \tilde{Q}_{MUT}}{\partial \alpha_{st}}\right)^2\left[\frac{u(\alpha_{st})}{\alpha_{st}}\right]^2 + \left(\frac{\kappa}{\tilde{Q}_{MUT}}\frac{\partial \tilde{Q}_{MUT}}{\partial \kappa}\right)^2\left[\frac{u(\kappa)}{\kappa}\right]^2
$$

(11)

Table 5. *Uncertainty budget for volumetric flow at MUT corresponding to Eq. (11)*

Vol. Flow; Q_{UMT} [lpm] Q_{MUT} = 113.56 lpm	Nom. Value [SI]	Rel. Unc. (k=1) [%]	Norm. Sen. Coeff. [ ]	Type A/B [ ]	Perc. Contrib. [%]	Comments
Volumetric Prover K-factor, K_{Vref}, [cm³/pul]	0.35442	0.037	1	B	99.1	Table 4
Duration of Stroke; Δt [s]	6.1	0.002	-1	B	0.3	Control Charts for freq. Calib.
Encoder Pules; N_e [pulse]	32410	0.000	1	B	0.0	Integer Number of Pulses
Temperature Encoder; Ten [°C]	23	0.017	0.0002	B	0.0	Environmental Sensor Calib. Records
Intial Fluid Temp., $Tcyl\_i$ [°C]	22	0.017	0.02	B	0.0	Temp. Cal. Records and spatial non-uniformity of 6 thermistors
Temperature at the MUT; T_{MUT} [°C]	21.75	0.017	-0.02	B	0.0	Temp. Cal. Records and spatial non-uniformity of 6 thermistors
Pressure at the MUT; P_{MUT} [kPa]	300	0.2	0.0003	B	0.0	Pres. Calib. Records
Pressure at the cylinder; $Pcyl\_i$ [kPa]	500	0.2	0.0005	B	0.0	Pres. Calib. Records
Linear Thermal expansion Coefficient of Stainless Steel; α_{st} [1/C]	1.7E-05	5	3E-05	B	0.0	CRC Handbook 73 Ed.
Isothermal Compressibility Factor; κ [1/kPa]	9.3E-07	7	0.0002	B	0.1	API Standard
Thermal Expan. Coeff., β [1/°C]	-0.00097	10	0.0002	B	0.4	Anton Paar Density Meas. Fit Residuals
Linear Thermal expansion Coefficient of Encoder; a_{en} [1/°C]	0.000008	5	1.6E-05	B	0.0	CRC Handbook 73 Ed.
RSS		**0.037**			**100**	

The expanded uncertainty in volumetric flow at the MUT is 0.074 %. As expected the majority of the uncertainty is attributed to the measurement of the volumetric prover K-factor. The uncertainty in mass flow is determined in an analogous fashion. The major contributing factor is the 0.015 % ($k = 1$) in Stoddard solvent desity. uncer

6. Comparison of Calibration data between the 20 L HLFS and other NIST flow standards

6.1 Calibration Procedure

To begin a calibration the MUT is installed in the test section, and the calibration fluid is pressured to the desired level. Next, an air bleed is performed to remove any air that entered the system during installation of the MUT. After the fluid and room temperatures are brought to equilibrium at T_{ref}, a custom software package is used to control the calibration process. Typical calibrations measure the flow at six set points at 5 %, 15 %, 30 %, 50 %, 70 %, 100 % of the full scale flow. Each of the six flows is measured on two occasions with 5 repeats on each occasion. The final calibration result for

each set point is the average of at least 10 measurements. The standard deviation of the 10 measurements is taken to be the reproducibility.

The calibration data for turbine meters is plotted in dimensionless units of Roshko number and Strouhal number. The Roshko number is

$$Ro = \frac{\mathcal{D}^2 f}{\nu} \qquad (12)$$

where f is the blade frequency, $\mathcal{D} = \mathcal{D}_{ref}\left[1 + \alpha_{st}\left(\tilde{T}_{MUT} - T_{ref}\right)\right]$ and $\nu = \left[1 + \nu_{ref}\left(\tilde{T}_{MUT} - T_{ref}\right)\right]$ is the kinematic viscosity. The Strouhal number is

$$St = \frac{\pi \mathcal{D}^3 f}{4 Q_{MUT}} \qquad (5c)$$

where flow is calculated via Eq. (9b).

6.2 Internal Comparison Results with other NIST flow standards

The uncertainty and consistency of the 20 L HLFS was verified by comparison to the other three liquid hydrocarbon standards in Table 1 using Stoddard solvent as the working fluid. In addition the 20 L HLFS was compared to the water flow facility which has an expanded uncertainty of 0.032%. A dual rotor turbine meter was used as the transfer standard for both of these comparisons. The standards were compared over a flow range from 3.8 lpm 151 lpm. The comparison results are plotted in Figure 5. The data shows all five of NIST's primary flow standards agreed within their uncertainties. In addition, the repeated calibrations of the turbine meter over a 6 month period demonstrates the stability of the 20 L HLFS.
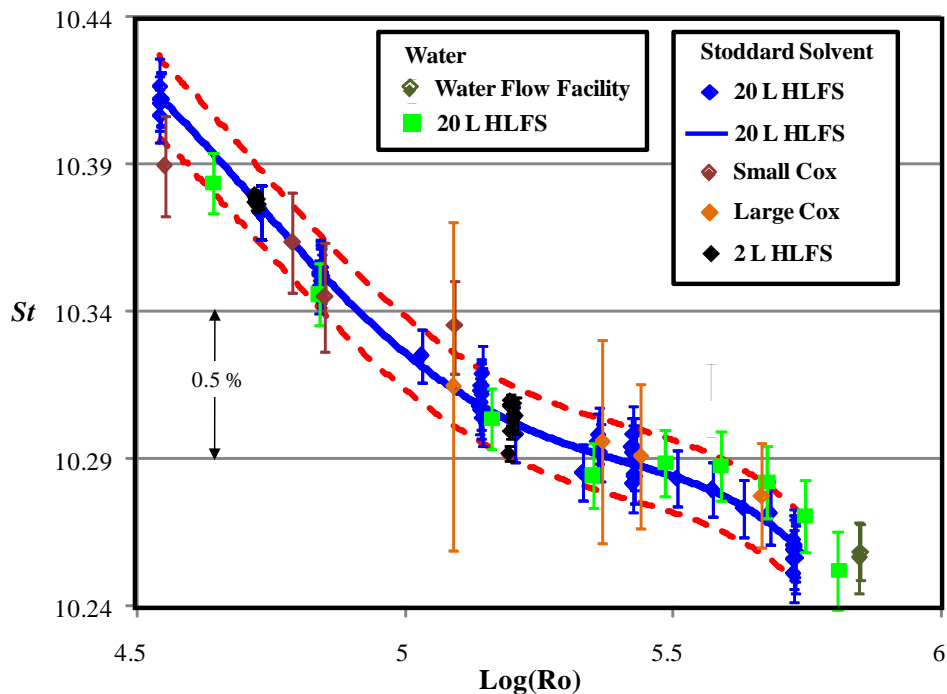
7. Summary and Conclusions

This manuscript documents the performance and uncertainty of NIST 20 L HLFS. This primary standard is used to provide flow traceability to NIST customers for hydrocarbon liquid flow. Based on the uncertainty analysis herein the standards uncertainty for volumetric flow is 0.074 % ($k = 2$) and the uncertainty for mass flow is 0.08 % ($k = 2$). The comparison of the 20 L HLFS with 3 other hydrocarbon liquid flow standards and a water flow standard demonstrates the derived uncertainty. In addition the comparison shows that all of the standards are in agreement within their stated uncertainties. Finally, the manuscript introduced a set of correction factors that can be used to estimate uncertainties of other liquid piston prover flow standards.

REFERENCES

[1] Yeh T. T., Aguilera, J., and Wright, J. D., *Hydrocarbon Liquid Calibration Service*, NIST Special Publication 250-1039, 2009.

[2] Yeh T. T., Aguilera, J., and Espina, P. I., Mattingly, G. E., Briggs, N. R., *An Uncertainty Analysis of A NIST Hydrocarbon Liquid Flow Calibration Facility*, Proceedings of Heat Transfer/Fluids Engineering Summer Conference, Charlotte, North Carolina, July 11-15, 2004.

[3] Shinder, I. I., and Moldover, M. R., *Dynamic Gravitational Standard for Liquid Flow: Model and Measurements*, 7th International Symposium on Fluid Flow Measurement, Anchorage, AK, August 12-14, 2009.

[4] Mattingly, G. E., *The Characterization of a Piston Displacement-Type Flowmeter Calibration Facility and the Calibration and Use of Pulsed Output Type Flowmeters*, Journal of Research of the National Institute of Standards and Technology, Vol. 97, No. 5, Pg. 509, September-October 1992.

[5] Coleman, H. W., and Steele, W. G., *Experimentation and Uncertainty Analysis for Engineers*, John Wiley and Sons, Inc., New York, NY, 1989

[6] Taylor, B. N. and Kuyatt C. E., *Guidelines for the Evaluating and Expressing the Uncertainty of NIST Measurement Results*, NIST TN-1297, MD,1994.Pressure vessel equation.

[7] Jaeger K. B., Davis R. S., *A Primer for Mass Metrology*, NBS (U.S.), Spec. Publ. 700-1, Industrial Measurement Series, 79 p. 5, 1984.

[8] Patterson, J. B. and Morris, E. C.*, Measurement of absolute water density, 1°C to 40°C*, Metrologia, 31, 277, 1994.